Journal of Molecular Structure 1248 (2022) 131451

Contents lists available at ScienceDirect

Journal of Molecular Structure

journal homepage: www.elsevier.com/locate/molstr

Rational design and synthesis of organic-inorganic hexavanadate hybrids with *p*-halogenated benzoyl ligands

Zhongwei Chen, Yu Wang, XingYue Wang, Zicheng Xiao*, Pingfan Wu*, Kanghong Hu*

Hubei University of Technology, Wuhan 430068, China

ARTICLE INFO

Article history:
Received 11 July 2021
Revised 2 September 2021
Accepted 4 September 2021
Available online 7 September 2021

Keywords:
Polyoxovanadate
Crystal structure
Synthesis mechanism
PyBOP

ABSTRACT

Three original hexavanadate-based materials $(DIEA)_2[V_6O_{13}\{(OCH_2)_3CNHCOC_6H_4X{-}p)\}_2]$ (X=Cl, Br, I) have been synthesized via the amidation of $H_2[V_6O_{13}\{(OCH_2)_3CNH_2\}_2]$ and *p*-halogenated benzoic acid. The components and structures of the products were determined by FT-IR, ^{1}H NMR, ESI-MS, XPS and single-crystal X-ray diffraction. The molecular structures of three compounds are similar: a Lindqvist-type cluster $\{V_6O_{19}\}$ covalently links to two halogenated benzoyl trialkoxyl ligands. However, they exhibit diverse packing manners because of their difference in hydrogen-bonding interactions. The anions $[V_6O_{13}\{(OCH_2)_3CNHCOC_6H_4Cl{-}p)\}_2]^{2-}$ are arranged in a 1D chain structure by intermolecular hydrogen-bonding interactions, while the other two compounds show a 2D "sandwich biscuit" layered packing structure without hydrogen bonds between the anions. Moreover, when choosing a condensing agent to increase the yield, PyBOP has an overwhelming advantage over common EDCI/HOBt. This article also discusses the reaction mechanism in detail, and provides experimental guidance for the rational design of POM-based organic-inorganic hybrids.

1. Introduction

Polyoxometalates (POMs) are nanoclusters with basic structural unit $[X_xM_yO_z]^{n-}$ (M = Mo, W, *V*, Nb, or Ta; X = *P*, Ti, Fe, Co, etc.) [1,2]. POMs have abundant structures and unique properties, which can be widely applied in catalysis, pharmacy, and material science [3–6]. Today, the research of POMs has expanded from pure inorganic chemistry to hybrid material chemistry [7]. The structural diversity and modifiable property make POM a perfect inorganic module for constructing inorganic-organic hybrid materials. By grafting appropriate organic groups, POMs can not only expand their structures and functions, but also adjust their properties and improve their performance in various applications, such as photoelectric materials, photocatalysts, and antitumor drugs [8,9]. In addition, POMs with active functional groups (such as amino or carboxylic group) can also be used as the basic reaction templates to build oligomers or network materials by further reacting with organic moieties.

Among various POMs, tris(hydroxymethyl)aminomethane (Tris−NH_2) functionalized POMs are regarded as a kind of important building blocks for the construction of complicated hybrid materials due to their accessibility and relatively high reactivity with organic ligands. To date, Tris−NH_2 has been successfully incorporated with Anderson-type polyoxomolybdate, Dawson-type heteropolytungstate and Lindqvist-type hexavanadate [10–13]. A number of hybrid materials with various structures and functions have been prepared through the post-functionalized POM platform [14–18]. Amidation is one of the most common reactions to connect the POM building blocks and the organic ligands [19–21]. Nevertheless, performing classical organic reactions on POMs is not an easy task. The complex chemical properties of POMs and the reduced activity of functional groups usually lead to low yields. The organic modification of Tris-functionalized POMs still needs further exploration and optimization.

In this article, we selected $H_2[V_6O_{13}\{(OCH_2)_3CNH_2\}_2]$ ($NH_2{-}V_6{-}NH_2$) as the basic structural unit to construct three hexavanadate hybrids $(DIEA)_2[V_6O_{13}\{(OCH_2)_3CNHCOC_6H_4X{-}p)\}_2]$ (X=Cl, Br, I corresponding to compounds 1, 2 and 3, respectively) through amidation. The structures of the products were fully characterized by FT-IR, 1H NMR, HR-ESI-MS, XPS, and single-crystal X-ray diffraction. Interestingly, we found that different reaction auxiliaries greatly affected the yields. When using PyBOP as the condensing agent and DIEA as the auxiliary base, the reaction yield can be significantly improved. The synthetic mechanisms of the two condensing agents were also discussed in detail.

* Corresponding authors.
E-mail addresses: zichxiao@hotmail.com (Z. Xiao), pingfanwu-111@163.com (P. Wu), hukh@hbut.edu.cn (K. Hu).

https://doi.org/10.1016/j.molstruc.2021.131451
0022-2860/

2. Experimental section

$NH_2-V_6-NH_2$ was firstly prepared according to previous literature [22]. Compounds 1–3 were obtained by dissolving a mixture of 0.5 mmol $NH_2-V_6-NH_2$, 1.2 mmol *p*-halogenated benzoic acid (4-chlorine benzoic acid, 4-bromine benzoic acid, and 4-iodine benzoic acid, respectively) and 1.2 mmol benzotriazole-1-yl-oxytripyrrolidinophosphonium hexafluorophosphate (PyBOP) in 50 mL anhydrous dimethylacetamide (DMAc). DIEA was added dropwisely to adjust the pH value to 7–8, and then the solution was heated at 55 °C and stirred for 24 h. After the reaction, the mixture was cooled down to room temperature and the insoluble solids were removed by the filtration. The crude products of compounds 1–3 were obtained as brown powder after the removal of the solvent by rotary evaporation. The powder was washed with ether several times and redissolved in acetonitrile. The insoluble impurities were removed by filtration and the crystals of the products were acquired by slow diffusion of *n*-butyl ether into the filtrate.

3. Results and discussions

3.1. Synthesis

Compounds 1–3 were all synthesized via the amidation of $NH_2-V_6-NH_2$ and *p*-halogenated benzoic acid. The condensing agent is the key to this reaction, which can activate carboxylic acid and significantly promote reaction efficiency. The frequently-used condensing agents for amidation are Dicyclohexylcarbodiimide (DCC), 1-ethyl-3(3-dimethylpropylamine) carbodiimide (EDCI) and PyBOP [23–25]. When the carbodiimide compounds (DCC or EDCI) were used as the condensing agent, the intermediates of the reaction are unstable and will transform to urea quickly. So condensing active agents, such as 1-hydroxybenzotriazole (HOBt) or 4-Dimethylaminopyridine (DMAP), are often used to produce more stable ester intermediates. DCC/HOBt condensing agent is not suitable for this reaction because it will generate insoluble urea byproducts, which are hard to wipe off. In this paper, we used two different condensing agents for comparison: EDCI/HOBt and PyBOP. The experiment results showed that the reaction with PyBOP had an overwhelming advantage in yield which was up to 80%, while that of EDCI/HOBt was only about 50%. This can be explained by the reaction mechanisms with the two different condensing agents. The plausible mechanisms of the reaction with EDCI/HOBt and PyBOP are shown in Figs. 1 and 2, respectively [26]. In both of the two mechanisms, the carboxylic acid is transformed into a benzotriazole ester, which is an active intermediate in the coupling reaction. When EDCI/HOBt is used as the condensing agent, EDCI is first protonated and then attacked by a carboxylic acid to form an acylisourea. The isourea group is then replaced by the HOBt anion, leading to a benzotriazole ester. When using PyBOP as the condensing agent [27], PyBOP first reacts with a carboxylic acid to form an acyloxyphosphonium salt, and then attacked by producing HOBt to form a benzotriazole ester. It is believed that the acyloxyphosphonium salt is less stable than acylisourea, and more active in the reaction with HOBt. Therefore, PyBOP shows higher efficiency than EDCI/HOBt in the amidation reaction.

Considering that the amidation reaction should be carried out under weakly alkaline conditions, we employed triethylamine and DIEA as an auxiliary base respectively. Finally, the DIEA was selected because it has weaker nucleophilicity and is less likely to attack carboxylic compounds. Thus there are fewer side reactions in the amidation process. Furthermore, DIEA can be easily protonated, so when EDCI/HOBt is used as the condensing agent, it may snatch the protons with EDCI, resulting in lower reaction efficiency. However, when PyBOP acted as the condensing agent, DIEA can directly involve in the reaction, avoiding the proton contention problem.

3.2. Spectroscopic characteristic

FT-IR, 1H NMR, HR-ESI-MS, and XPS were used to characterize the molecular structure of the products. Fourier Transform Infrared spectroscopy (FT-IR) is a very essential structure specification technique that arises from radiation interactions and molecular vibrations. As shown in Figs. S1 and S2, all three compounds show strong absorption bands near 960 cm^{-1}, 806 cm^{-1}, and 711 cm^{-1} originating from the stretching vibration between vanadium–oxygen bonds, (vas (V−Ot), vas (V−Ob), and vas (V−O alkoxy), respectively), which can also be seen in the IR spectrum of $NH_2-V_6-NH_2$. It illustrates that the derived hexavanadate hybrids still maintain their parent structure after the reaction. The vibration bands of DIEA cations are located near 2956 cm^{-1} (vas (CH_3)), 2873 cm^{-1} (vas (CH_3)) and the wide peak around 3450 cm^{-1} is the stretching vibration of N−H. The absorption peaks from 1600 cm^{-1} to 1400 cm^{-1} are attributed to the benzene rings, while the strong peak around 1680 cm^{-1} corresponds to the stretching vibration of the amidic C=O bond. These emerging peaks demonstrate that the amino groups in $NH_2-V_6-NH_2$ have been acylated successfully. The HR-ESI-MS of compounds 1–3 only show m/z peaks at 1026.68431, 1116.58115 and 1210.55749, corresponding to the theory of the anions $H[V_6O_{13}\{(OCH_2)_3CNHCOC_6H_4Cl-p)\}_2]^{2-}$ (theoretical value 1026.67299), $[V_6O_{13}\{(OCH_2)_3CNHCOC_6H_4Br-p)\}_2]^{2-}$ (theoretical value 1116.56992) and $[V_6O_{13}\{(OCH_2)_3CNHCOC_6H_4I-p)\}_2]^{2-}$ (theoretical value 1210.54422) respectively. These results also support the assumed structures.

X-ray photoelectron spectroscopy (XPS) can not only verify the elementary composition of a compound, but also judge the valence states of atoms according to the binding energies. The XPS spectra of compounds 1–3 are shown in Figs. S6–S8. The elaborate vanadium spectra of all the three compounds can be fitted into two peaks with the binding energies around 524.0 eV ($V_{2p1/2}$) and 517.0 eV ($V_{2p3/2}$), respectively. According to the correlation spectra of vanadium atoms reported in the literature, it can be concluded that all vanadium atoms in the products are in the highest valence state (+5) [28]. These results are consistent with the valence state of vanadium in $NH_2-V_6-NH_2$, indicating that the metal valence state remains the same after being covalently attached to halogenated benzoic acids. The existence of halogen atoms in compounds 1–3 can also be confirmed by the XPS spectra. For compound 1, the peaks of the chlorine atoms is located at 202.0eV ($Cl_{2p1/2}$) and 200.4eV ($Cl_{2p3/2}$). The peaks of bromine and iodine atoms can be found at 70.6 eV (Br3d5/2) for compound 2 and 620.5 eV ($I_{3d5/2}$) for compound 3, respectively. These peaks are all consistent with the standard spectrogram, indicating that 4-chlorobenzoic acid, 4-bromobenzoic acid, and 4-iodobenzoic acid have been successfully introduced into the hexavanadate.

3.3. Molecular structure

The molecular structures of the three derivatives were further confirmed by single-crystal X-ray diffraction. All these structures are composed of one $[V_6O_{13}\{(OCH)_3CNHOCC_6H_4X\}_2]^{2-}$ (X = Cl, Br, *I*) anion and two DIEA cations. Compounds 2 and 3 both crystallize in a monoclinic system, space group *P21/c* with similar cell parameters, while compound 1 crystallizes in a triclinic system with space group symmetry *P-1* (Table 1). As shown in Fig. 3, the anions of all the compounds represent a rod-like architecture which consisted of a Lindqvist-type hexavanadate cluster $\{V_6O_{19}\}$ with two rigid Tris ligands occupying the opposite sides of the octahedron. The *p*-halobenzoyl groups in compounds 1–3 are covalently

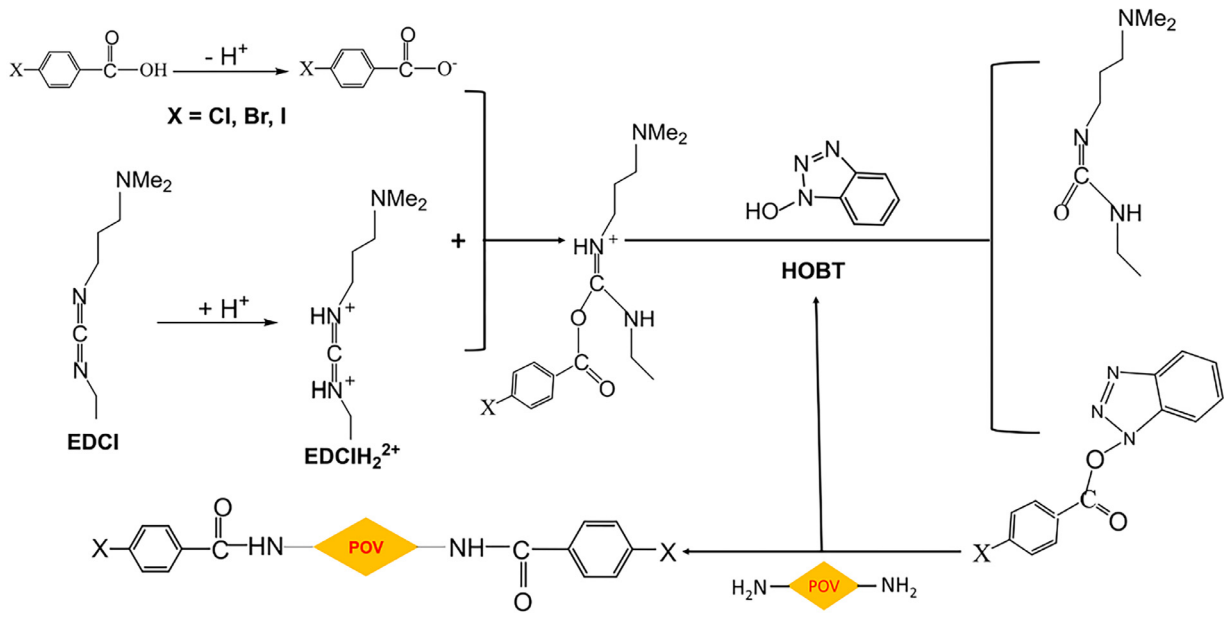

Fig. 1. The synthesis mechanism using EDCI/HOBt as the condensing agent.

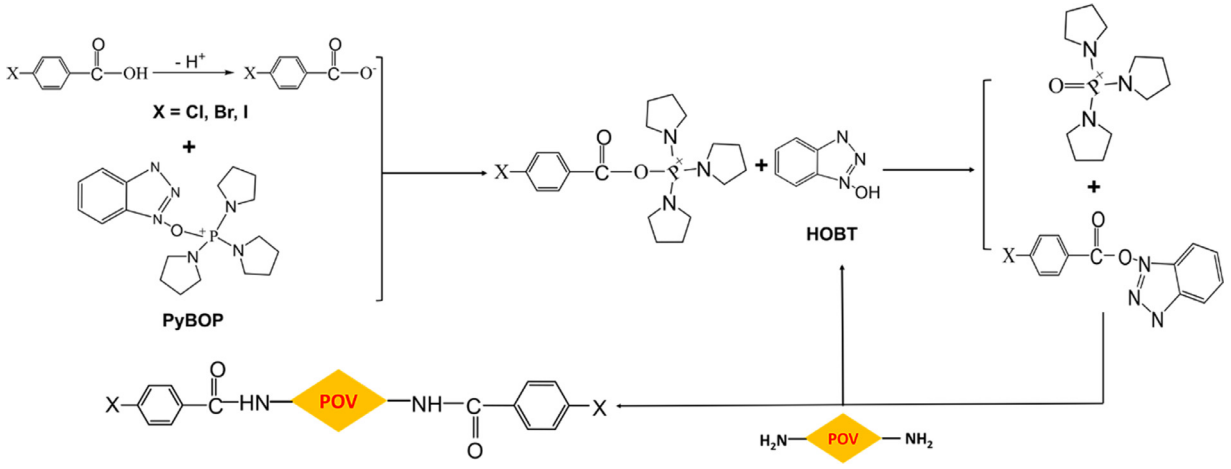

Fig. 2. The synthesis mechanism using PyBOP as the condensing agent.

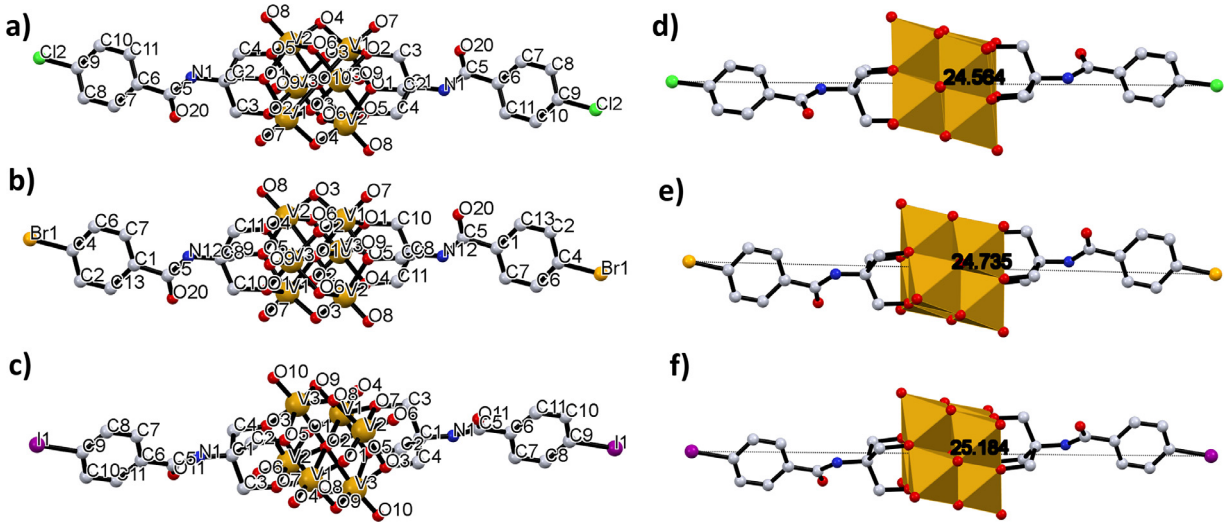

Fig. 3. Anion structures with atomic labels of compounds 1 (a). 2 (b) and 3 (c). The total distances of compound 1 (e); compound 2 (f) and compound 3 (g). Red spheres: O atoms; orange sphere: V atoms; white sphere: C atoms; blue sphere: H atoms; green spheres: Cl atoms; brown spheres: Br atoms; purple sphere: I atoms; light blue spheres: H atoms.

Table 1
single-crystal diffraction data of compounds 1–3.

Compound	1	2	3
Empirical formula	$C_{42}H_{60}Cl_2N_6O_{21}V_6$	$C_{46}H_{80}Br_2N_6O_{23}V_6$	$C_{46}H_{80}I_2N_6O_{23}V_6$
Formula weight	1361.5	1550.62	1644.60
T/K	296.15	273.15	100(2)
Crystal system	triclinic	monoclinic	monoclinic
Space group	*P - 1*	$P2_1/c$	$P2_1/c$
a/Å	10.1866(10)	15.608(2)	15.7035(15)
b/Å	12.0553(10)	10.4961(15)	10.5511(10)
c/Å	12.4333(12)	19.455(3)	19.3560(18)
α/°	108.712(2)	90	90
β/°	102.984(3)	105.794(5)	106.2920(10)
γ/°	90.914(3)	90	90
Volume/Å^3	1402.7(2)	3066.8(8)	3078.3(5)
Z	1	2	2
ρ calc g/cm^3	1.612	1.679	1.774
μ/mm^{-1}	1.132	2.259	1.956
F(000)	694	1580	1652
Crystal size/mm^3	0.28× 0.26 × 0.24	0.26 × 0.24 × 0.15	0.33 × 0.30 × 0.15
2Θ range for data collection/°	4.122 to 55.344°	4.352 to 53.424°	4.384 to 57.998°
Index ranges	$-13 \le h \le 13$	$-19 \le h \le 18$	$-21 \le h \le 21$
	$-15 \le k \le 15$	$-13 \le k \le 12$	$-14 \le k \le 14$
	$-9 \le l \le 16$	$-19 \le l \le 22$	$-22 \le l \le 26$
Reflections collected	12441	16610	28608
Independent reflections	$R_{int} = 0.0405$	$R_{int} = 0.0492$	$R_{int} = 0.0473$
	$R_{sigma} = 0.0759$	$R_{sigma} = 0.0719$	$R_{sigma} = 0.0416$
Data/restraints/parameters	6512/0/355	5709/46/382	8148/0/384
GOF on F^2	1.043	1.046	1.06
Final R indexes [$I >= 2\sigma$ (I)]	$R_1 = 0.0528$	$R_1 = 0.0604$	$R_1 = 0.0512$
	$wR_2 = 0.1226$	$wR_2 = 0.1421$	$wR_2 = 0.1333$
Final R indexes [all data]	$R_1 = 0.0873$	$R_1 = 0.1080$	$R_1 = 0.0630$
	$wR_2 = 0.1356$	$wR_2 = 0.1635$	$wR_2 = 0.1417$
Largest diff. peak/hole /e Å^3	0.80/-0.43	1.04/-0.59	2.87/-2.41

attached to the Tris ligands via amidic C–N bond with an approximate distance of 1.34 Å. The total lengths of the three anions are 24.584 Å, 24.735 Å, and 25.184 Å, respectively. The main reason for this difference is the atomic radius of halogen atoms as well as the atom electronegativity. Among the three halogen atoms, the chlorine atom has the smallest atomic radius and greatest electronegativity which results in the shortest C−X bond length. The bond distances and angles of the three compounds were shown in Table S2–S7.

In the crystal structures of compounds 1–3, there are hydrogen-bonding interactions originated from the ammonium hydrogen of the cation and the bridging oxygen of the $\{V_6O_{19}\}$ cluster (N3−H···O3$^{\#}$, 3.013 Å in compound 1; N1−H···O3$^{\#}$, 2.847 Å in compound 2; N2−H···O8$^{\#}$, 2.825 Å in compound 3). However, compound 1 also shows hydrogen bonds between the amidic hydrogen and the terminal oxygen of the adjacent polyanion (N1−H···O8$^{\#}$, 3.193 Å), while compounds 2 and 3 have no hydrogen-bonding interaction between the anions. The difference in hydrogen bonding also affects the crystal packing behavior. As shown in Fig. 4, compound 1 presents a 1D chain arrangement in the crystal structure, and all the anions in the crystal cell are parallel. viewed from the *a* axis, compounds 2 and 3 show a 2D layered packing structure similar to “sandwich biscuit”, and the polyanions from the neighboring layers are almost perpendicular.

In our previous report, we discovered that the Lindqvist-type hexavanadate with halogen organic ligands $[V_6O_{13}\{(OCH_2)_3CCH_2OOCCH_2CH_2CONHC_6H_4X-p)\}_2]^{2-}$ (X=Cl, Br, I) formed strong halogen-bonding interactions between the halogen atom and the terminal oxygen of the hexavanadate cluster [29]. However, in this work, compounds 1–3 do not form any halogen-bonding interactions. The plausible reason may lie in the rigid organic ligands in these compounds. Since the formation of halogen bonds has a strict directional requirement, the short and rigid organic ligands in compounds 1–3 are adverse to adjusting the relative position of halogen and oxygen atoms, thereby hindering the formation of halogen bonds.

4. Conclusion

In this article, three organic-inorganic hybrids of Lindqvist-type hexavanadate with *p*-halogenated benzoyl ligands have been successfully prepared, and their structures have been fully characterized by FT-IR, 1H NMR, ESI-MS, XPS, and single-crystal XRD. We employed different condensing agents in the synthesis and found that PyBOP showed a higher yield than EDCI/HOBt. This result is explained by the reaction mechanism, and indicates that PyBOP is a better condensing agent than carbodiimides in the scheme of amidation and functionalization of POMs. These three compounds show different packing manners, which are properly originated from their differences in hydrogen-bonding interactions. Moreover, unlike our previous reported hexavanadates with halogenated organic ligands, there is no halogen-bonding interaction in compounds 1–3, indicating that it is difficult for POMs with rigid organic ligands to form intermolecular halogen bonds. These results provide a reference case for the design of the novel POM-based supramolecular materials.

Supplementary data

The experimental details, spectroscopic data (FT-IR, ESI-MS and XPS) and tables of bond lengths and angles are given in Supporting Information. Crystallographic data for compounds 1–3 have been deposited with the Cambridge Crystallographic Data Centre (CCDC number 2095753, 2095754 and 1870179, respectively). The data can be obtained free of charge from the Cambridge Crystallographic Data Centre *via* www.ccdc.cam.ac.uk/data_request/cif.

Declaration of Competing Interest

There is no financial or non-financial assistance provided by a third party for the reported work. There is no inancial interest or

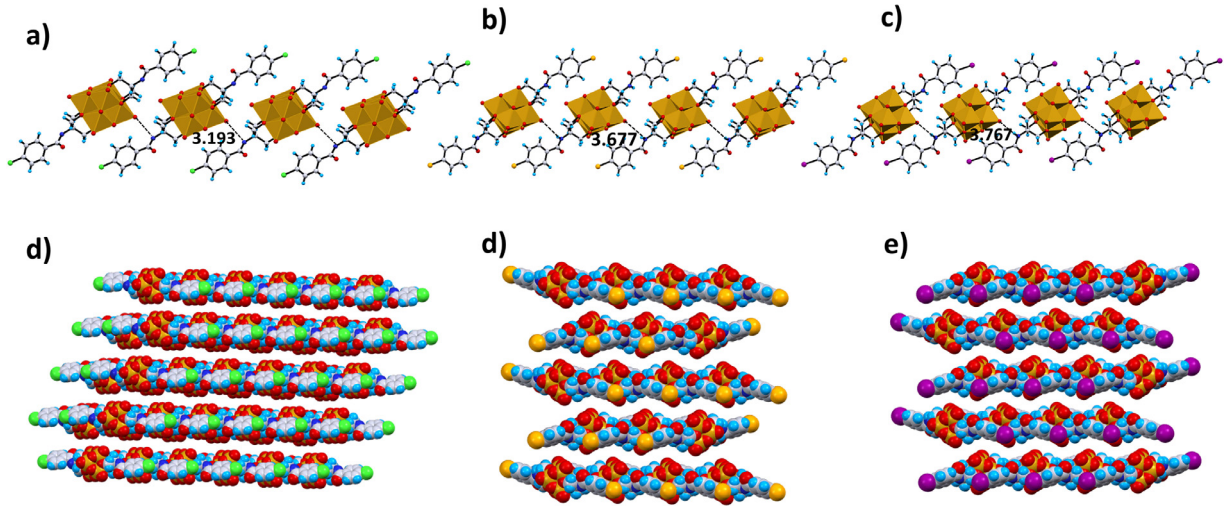

Fig. 4. Molecule hydrogen bond interaction for compound 1 (a) compound 2 (b) and compound 3 (c); the packing diagrams for compound 1 (e) compound 2 (f) and compound 3 (g).

relationship related to the subject matter within the last 3 years. There is no any patents or copyrights. Authors have no conflict of interest to declare.

CRediT authorship contribution statement

Zhongwei Chen: Investigation, Writing – original draft. **Yu Wang:** Data curation, Writing – review & editing, Visualization. **XingYue Wang:** Data curation, Validation. **Zicheng Xiao:** Methodology, Formal analysis, Writing – review & editing, Funding acquisition. **Pingfan Wu:** Supervision, Writing – review & editing, Funding acquisition. **Kanghong Hu:** Conceptualization, Supervision, Project administration.

Acknowledgment

This work is supported by National Natural Science Foundation of China (No. 21271068, 21401050).

Supplementary materials

Supplementary material associated with this article can be found, in the online version, at doi:10.1016/j.molstruc.2021.131451.

Reference

[1] M.A. Teplonogova, A.D. Yapryntsev, A.E. Baranchikov, V.K. Ivanov, Selective hydrothermal synthesis of ammonium vanadates(V) and (IV,V), Transit. Metal Chem. 44 (2019) 25–30.
[2] Z. Zhang, Y.L. Wang, Y. Liu, S.L. Huang, G.Y. Yang, Three ring-shaped Zr(iv)-substituted silicotungstates: syntheses, structures and their properties, Nanoscale 12 (2020) 18333–18341.
[3] K. Tandekar, P. Naulakha, S. Supriya, Reversible redox activity of $\{Mo_{72}Fe_{30}\}$ nano-polyoxometalate cluster in three crystalline forms, Inorg. Chim. Acta 511 (2020) 119729.
[4] C. Pimpao, I.V. da Silva, A.F. Mosca, J.O. Pinho, M.M. Gaspar, N.I. Gumerova, A. Rompel, M. Aureliano, G. Soveral, The aquaporin-3-inhibiting potential of polyoxotungstates, Int. J. Mol. Sci. 21 (2020) 2467.
[5] Y. Gu, Q. Li, Y. Huang, Y. Zhu, Y. Wei, L. Ruhlmann, Polyoxovanadate-iodobodipy supramolecular assemblies: new agents for high efficiency cancer photochemotherapy, Chem. Commun. 56 (2020) 2869–2872.
[6] C. Wang, C.Y. Zhu, M. Zhang, Y. Geng, Y.G. Li, Z.M. Su, An intriguing window opened by a metallic two-dimensional Lindqvist-cobaltporphyrin organic framework as an electrochemical catalyst for the CO_2 reduction reaction, J. Mater. Chem. A 8 (2020) 14807–14814.
[7] A.V. Anyushin, A. Kondinski, T.N. Parac-Vogt, Hybrid polyoxometalates as post-functionalization platforms: from fundamentals to emerging applications, Chem. Soc. Rev. 49 (2020) 382–432.
[8] E. Schreiber, N.A. Hartley, W.W. Brennessel, T.R. Cook, J.R. McKone, E.M. Matson, An organofunctionalized polyoxovanadium cluster as a molecular model of interfacial pseudocapacitance, ACS Appl. Energy Mater. 2 (2019) 8985–8993.
[9] Y. Luo, S. Maloul, S. Schoenweiz, M. Waechtler, C. Streb, B. Dietzek, Yield-not only lifetime-of the photoinduced charge-separated state in iridium complex-polyoxometalate dyads impact their hydrogen evolution reactivity, Chem. A Eur. J. 26 (2020) 8045–8052.
[10] R. Delmont, B. Hasenknopf, P. Herson, P. Gouzerh, Anderson-type heteropolymolybdates containing tris(alkoxo) ligands: synthesis and structural characterization, Eur. J. Inorg. Chem. 2002 (2002) 1081–1087.
[11] C. Peng, T. Chen, B. Zeng, G. Chen, C. Yuan, Y. Xu, L. Dai, Anderson-type polyoxometalate-based hybrid with high flame retardant efficiency for the preparation of multifunctional epoxy resin nanocomposites, Compos. Part B Eng. 186 (2020) 107780.
[12] Y. Zhu, Y. Huang, Q. Li, D. Zang, J. Gu, Y. Tang, Y. Wei, Polyoxometalate-based photoactive hybrid: uncover the first crystal structure of covalently linked hexavanadate-porphyrin molecule, Inorg. Chem. 59 (2020) 2575–2583.
[13] C.P. Pradeep, D.L. Long, G.N. Newton, Y.F. Song, L. Cronin, Supramolecular metal oxides: programme hierarchical assembly of a protein-sized 21kDa $[(C_{16}H_{36}N)_{19}\{H_2NC(CH_2O)_3P_2V_3W_{15}O_{59}\}_4]^{5-}$ polyoxometalate assembly, Angew. Chem. Int. Ed. 47 (2008) 4388–4391.
[14] Y. Wang, X.J. Lin, B. Huang, W.Z. Chen, Z.C. Xiao, P.F. Wu, The crystal packing, morphology and hydrophobicity of polyoxometalate-based amphiphilic materials, CrystEngComm 22 (2020) 2434–2438.
[15] Y.T. Zhu, Y.C. Huang, Q. Li, D.J. Zang, J. Gu, Y.J. Tang, Y.G. Wei, Polyoxometalate-based photoactive hybrid: uncover the first crystal structure of covalently linked hexavanadate-porphyrin molecule, Inorg. Chem. 59 (2020) 2575–2583.
[16] X.X. Li, Y.X. Wang, R.H. Wang, C.Y. Cui, C.B. Tian, G.Y. Yang, Designed assembly of heterometallic cluster organic frameworks based on Anderson-type polyoxometalate clusters, Angew. Chem. Int. Ed. 55 (2016) 6462–6466.
[17] Y.C. Ji, J. Hu, L.J. Huang, W. Chen, C. Streb, Y.F. Song, Covalent attachment of Anderson-type polyoxometalates to single-walled carbon nanotubes gives enhanced performance electrodes for lithium ion batteries, Chem. A Eur. J. 21 (2015) 6469–6474.
[18] A. Iqbal, H.M. Asif, Y.S. Zhou, L.J. Zhang, T. Wang, F.K. Shehzad, X.Y. Ren, From simplicity to complexity in grafting Dawson-type polyoxometalates on porphyrin, leading to the formation of new organic–inorganic hybrids for the investigation of third-order optical nonlinearities, Inorg. Chem. 58 (2019) 8763–8774.
[19] F.d. Azambuja, T.N. Parac-Vogt, Water-tolerant and atom economical amide bond formation by metal-substituted polyoxometalate catalysts, ACS Catal. 9 (2019) 10245–10252.
[20] T. Minato, K. Suzuki, K. Yamaguchi, N. Mizuno, Alkoxides of trivacant lacunary polyoxometalates, Chem. A Eur. J. 23 (2017) 14213–14220.
[21] V. Kalyani, V.S.V. Satyanarayana, A.S. Sarkar, A. Kumar, S.K. Pal, S. Ghosh, K.E. Gonsalves, C.P. Pradeep, A radiation sensitive hybrid polymer based on an Mn-Anderson polyoxometalate cluster and a UV active organic monomer: synergistic effects lead to improved photocurrent in a photoresponse devic, RSC Adv. 5 (2015) 36727–36731.
[22] A. Bayaguud, K. Chen, Y. Wei, Facile synthesis of an organically-derivatized hexavanadate containing the remote amino group, $TBA_2[V_6O_{13}\{(OCH_2)_3CNH_2\}_2]$, CrystEngComm 18 (2016) 4042–4045.
[23] X. Hu, H. Wang, B. Huang, N. Li, K. Hu, B. Wu, Z.C. Xiao, Y.G. Wei, P.F. Wu, A new scheme for rational design and synthesis of polyoxovanadate hybrids with high antitumor activities, J. Inorg. Biochem. 193 (2019) 130–132.

[24] Z.C. Xiao, B. Huang, S. Xu, X.L. Hu, P. F.Wu, Polyoxovanadate-based inorganic-organic derivatives synthesized by the activation of NHS intermediate at room temperature, ChemistrySelect 4 (2019) 1742–1744.
[25] Y. Wang, X.J. Lin, B. Huang, W.Z. Chen, Z.C. Xiao, P.F. Wu, The crystal packing, morphology and hydrophobicity of polyoxometalate-based amphiphilic materials, CrystEngComm 22 (2020) 2434–2438.
[26] L.C. Chan, B.G. Cox, Kinetics of amide formation through carbodiimide/*N*-hydroxybenzotriazole (HOBt) couplings, J. Org. Chem. 72 (2007) 8863–8869.
[27] T. Hoeg-Jensen, M.H. Jakobsen, C.E. Olsena, A. Holm, Formation of peptide thioamides by use of fmoc amino monochioacid and PyBOP, Tetrahedron Letters 132 (1991) 7617–7620.
[28] B. Huang, D.G. Ke, Z.L. Xiong, Y. Wang, K. Hu, P. Jiang, M.H. Liang, Z.C. Xiao, P.F. Wu, Covalent hybrid materials between polyoxometalates and organic molecules for enhanced electrochemical properties, J. Mater. Sci. 55 (2020) 5554–5570.
[29] X.J. Lin, B. Huang, Z.L. Xiong, T. Fang, X. Zhang, Z.C. Xiao, P.F. Wu, Supramolecular architectures of polyoxometalate hybrids originating from halogen and hydrogen-bonding interactions, ChemistrySelect 3 (2018) 11008–11011.